Field-induced spin splitting and anomalous photoluminescence circular polarization in CH_{3}NH_{3}PbI_{3} films at high magnetic field

Chuang Zhang, Dali Sun, Zhi-Gang Yu, Chuan-Xiang Sheng, Stephen McGill, Dmitry Semenov, and Zeev Valy Vardeny

Phys. Rev. B **97**, 134412 — Published 16 April 2018

DOI: 10.1103/PhysRevB.97.134412

Field-induced spin splitting and anomalous photoluminescence circular polarization in $CH_3NH_3PbI_3$ films at high magnetic field

Chuang Zhang[1,†], Dali Sun[1,2,†], Zhi-Gang Yu[3], Chuan-Xiang Sheng[1], Stephen McGill[4], Dmitry Semenov[4], Zeev Valy Vardeny[1,*]

[1]*Department of Physics and Astronomy, University of Utah, Salt Lake City, Utah 84112, USA*

[2]*Department of Physics, North Carolina State University, Raleigh, North Carolina 27695, USA*

[3]*ISP/Applied Sciences Laboratory, Washington State University, Spokane, Washington 99210, USA*

[4]*National High Magnetic Field Laboratory, Tallahassee, Florida 32310, USA*

Abstract

The organic-inorganic hybrid perovskites show excellent optical and electrical properties for photovoltaic and a myriad of other optoelectronics applications. Using high-field magneto-optical measurements up to 17.5 Tesla at cryogenic temperatures, we have studied the spin-dependent optical transitions in the prototype $CH_3NH_3PbI_3$, which are manifested in the field-induced circularly polarized photoluminescence emission. The energy splitting between left and right circularly polarized emission bands is measured to be ~1.5 meV at 17.5 Tesla, from which we obtained an exciton effective *g*-factor of ~1.32. Also from the photoluminescence diamagnetic shift we estimate the exciton binding energy to be ~17 meV at low temperature. Surprisingly, the corresponding field-induced circular polarization is 'anomalous' in that the photoluminescence emission of the higher split energy band is stronger than that of the lower split band. This 'reversed' intensity ratio originates from the combination of long electron spin relaxation time and hole negative *g*-factor in $CH_3NH_3PbI_3$, which are in agreement with a model based on the **k·p** effective-mass approximation.

*Corresponding author: val@physics.utah.edu.

[†]These authors contributed equally to this work.

Organometallic lead halide perovskites are fascinating solution-processed semiconductors because of their excellent charge transport and luminescent properties that are imperative for optoelectronic device applications.[1-4] In addition, it has been noticed that the spin-orbit coupling (SOC) plays an important role in the electronic structure of this class of hybrid organic-inorganic materials.[5-8] The strong SOC caused by the lead and halogen heavy atoms also provides the means of controlling the spin degree of freedom, which is lacking in traditional organic semiconductors. Consequently spin-related phenomena such as magnetic field effect,[9,10] inverse spin Hall effect,[11,12] Rashba spin splitting,[14-17] optically spin injection[18] and spin-selective optical Stark effect[19] have been theoretically predicted and experimentally demonstrated in two- and three-dimensional hybrid perovskites. These recent breakthroughs illustrate that the organic-inorganic perovskites hold great potential in spin manipulation which is required for spintronic applications.[20] High-field magneto-optics[21-23] and polarization spectroscopy[24] studies have been carried out to elucidate the spin-related electronic band structure in inorganic perovskite nanocrystals.

The method of magnetic field-induced circular polarization (FICPO) has been a powerful tool in studying the spin-dependent transitions in semiconductors.[25-28] The external field introduces an energy splitting between the spin sublevels of the material, which in many cases results in circularly polarized absorption and/or emission. As $CH_3NH_3PbI_3$ has a similar but reversed band structure to that of GaAs, (namely S= ½ and L=0 valance band and S = ½ L=1 conduction band that further splits into two bands with J=1/2 and J=3/2), the FICPO technique is expected to reveal the spin properties of photoexcitations in this material too. Indeed high field magneto-absorption was carried out by Miura *et al*.[29,30] in few hybrid perovskites which showed a clear Zeeman splitting effect of excitons, from which they obtained the exciton *g*-factors and diamagnetic shifts. More recently Nicholas *et al*. observed Landau levels splitting at high magnetic field from which they obtained the exciton binding energies in methylammonium/formamidinium hybrid perovskite.[31,32] In addition, the band structure and exciton levels of these materials have been investigated theoretically,[33-35] providing useful information that has helped understanding the circular polarization of optical transitions in these compounds upon the application of magnetic field.

The radiative recombination between spin polarized electrons in the conduction band (CB) and holes in the valence band (VB) leads to left-(σ-) and right-(σ+) circularly polarized photo respectively according to the optical selection rules. Consequently, under an applied magnetic field having strength *B*, the two oppositely circularly polarized PL bands split by the Zeeman energy, $\Delta E(B)$.[36] In addition, if thermal equilibrium is reached before recombination sets in, the induced difference between the photoexcitation populations of the two energy-split spin states would cause intensity imbalance between the two polarized emission bands. Because the Zeeman energy ΔE increases with *B*, the σ- and σ+ emissions would gradually split and shift with *B* providing a direct measurement of the exciton effective *g*-factor, diamagnetic shift coefficient, c_0, and other important physical parameters[37] of the photoexcitations in the perovskites.

In this work we obtained strong circular polarization of the PL emission in polycrystalline $CH_3NH_3PbI_3$ thin films induced by high magnetic field at cryogenic temperatures using light excitation with linear polarization. We measured field induced Zeeman energy splitting, $\Delta E(B)$ as large as ~1.5 meV at 17.5 Tesla that shows linear dependence on *B*, from which we extract an effective *g*-factor of 1.32 for the excitons in $CH_3NH_3PbI_3$. An exciton diamagnetic shift in the PL emission energy has been also measured, from which we obtained a coefficient $c_0=0.9\times10^{-5}$ eV/T^2, and exciton binding energy E_B=17 meV in the orthorhombic $CH_3NH_3PbI_3$ phase. We also observed a FICPO value of up to 20% at 10 K which decreased with the temperature based on the competition between spin/thermal relaxation and radiative recombination. However the obtained FICPO was 'opposite' to the normal Boltzmann distribution; namely the PL intensity is stronger for the spin sublevel with the higher energy. This anomalous FICPO originates from a combination of *negative g-factor* for holes in the VB and their shorter spin lattice relaxation time than that of the electrons in the CB, in agreement with the k·p effective-mass model approximation for $CH_3NH_3PbI_3$.[38] Our work complement the high-field magneto-absorption results,[29-32] and the transient spin dynamics measurement using picosecond transient Kerr rotation,[39] by providing a steady-state PL method that illustrates the spin-selective optical processes[40] upon the effect of strong SOC in the hybrid perovskites.

The $CH_3NH_3PbI_3$ polycrystalline film was prepared via one-step spin-casting method.[41] For the FICPO measurements, the $CH_3NH_3PbI_3$ film was placed in a liquid helium cryostat (4-150 K), and the magnetic field was provided by a superconducting magnet up to ~17.5 T (MagLab, SCM-3). As shown in Fig. 1a, a solid-state laser operating at 486 nm was coupled into a fiber used as the pump excitation from the substrate side, whereas the PL emission was collected in free space and measured with a fiber spectrometer (Ocean Optics USB 4000). The optical setup was set in the Faraday configuration, in which the excitation and emission beams were aligned along the *B* direction, which is perpendicular to the film plane. The PL emission was separated into σ- and σ+ components using a broadband quarter-wave plate (400-800 nm, Thorlabs) followed by a linear polarizer. The experimental apparatus was calibrated with an unpolarized light source, from which we obtained a systematic error <0.2% in measuring the circular light polarization.

When the $CH_3NH_3PbI_3$ film is excited above the optical gap, electrons in the CB and holes in the VB are photogenerated as shown in Fig. 1b. After ultrafast hot carrier thermalization[42] the photogenerated electrons and holes form Coulomb bounded e-h pairs that lead to excitons, especially at low temperatures since the exciton binding energy, E_B is of order of tens meV (see below). Subsequently PL is generated from free excitons, excitons coupled to phonons (namely 'phonon replica'), and excitons trapped in native defects (defect-related PL).[43,44] Indeed the PL spectrum of $CH_3NH_3PbI_3$ film at 4 K (Fig. 1c) shows strong PL emission in the near infrared spectral range, which can be decomposed into three Lorentzian spectral components. The free exciton emission appears at 770.5 nm (or 1.609 eV), whereas the 'phonon replica' is at 777.7 nm (or 1.594 eV) that is 15 meV apart; this is attributed to the strongly coupled longitudinal optical phonon mode at ~15 meV.[45] This decomposition also explains the observed asymmetry of the main PL band towards the red. The third PL component is due to defect-related emission at 803.6 nm (or 1.543 eV). The native defects in this case may be reminiscences from the high-temperature tetragonal phase in the host of low-temperature orthorhombic phase,[46] which are trapped upon cooling the sample from room temperature to 4 K. This defect state is ~65 meV lower than that of the free exciton, and serves as a native defect which may efficiently trap free excitons at low temperature.

Following thermalization the photogenerated electrons occupy the lowest CB bottom characterized by J = 1/2 (the higher CBs with J=3/2 are split from the J=1/2 CB by the strong SOC in this material) and symmetrically the holes reach the VB top characterized by S = 1/2. The optical transitions between the CB bottom and VB top are considered to be between two spin 1/2 quasiparticles, as shown in Fig. 2a. Consequently the recombination of the spin-polarized carriers with $\Delta J=\pm 1$ and $\Delta m=\pm 1$ correspond to the σ- and σ+ circularly polarized PL emission.[25] Without an applied external magnetic field the two σ- and σ+ emission bands are degenerate, as shown in Fig. 2b. In contrast, at $B>0$ this degeneracy is lifted due to the Zeeman interaction, where the exciton energy, E is expressed by;

$$E(B)_{\pm} = E_0 \pm \frac{1}{2} g\mu_B B + c_0 B^2 \qquad (1)$$

Here g is an effective Landé g-factor, μ_B is the Bohr magneton, and c_0 is so-called diamagnetic coefficient. This creates an energy splitting between the σ- and σ+ emission bands and a shift of the average emission energy. As seen in Fig. 2b the energy splits by nearly 1 nm between σ- and σ+ emission bands at B=17.5 T. We note that the splitting due to the Zeeman term, $g\mu_B B$ is linear with B and therefore the g-factor can be extracted from the slope with high accuracy. The diamagnetic shift, $c_0 B^2$ could be also extracted from the blue shift of the average PL emission band with B.

By composing the σ- and σ+ emission bands at different fields, we plot the central wavelengths of the free exciton emission band vs. B in Fig. 2c. The accompanied 'phonon replica' emission band behaves similarly; whereas the trapped exciton band shows very little shift or split (see Fig. S1).[41] We first analyze the diamagnetic shift. From a fit to the PL average spectrum using a parabolic shift, $c_0 B^2$, we obtain $c_0=0.9\times10^{-5}$ eV/T^2 in $CH_3NH_3PbI_3$ (see Fig. S2),[41] which is similar to that obtained in III-V semiconductors.[37] Consequently, we use the traditional relation $\boldsymbol{c_0 = \frac{\hbar^4 \varepsilon^2}{4e^2\mu^3}}$, where ħ is the reduced Planck constant, ε is the relative dielectric constant, e is the elementary charge, and μ is the exciton reduced mass. Using this relation and $\mu=0.104m_e$[31] we obtain ε=9.1 for $CH_3NH_3PbI_3$, and the deviation from its high-frequency dielectric constant (ε_∞=6.5) is due to exciton screening by polar phonons.[35] From our estimated ε value we may evaluate

the exciton binding energy, E_B using the relation $\boldsymbol{E_B = \frac{e^4 \mu}{2\hbar^2 \varepsilon^2}}$. We get E_B ~17 meV in the orthorhombic $CH_3NH_3PbI_3$ phase, which is very close to the previous estimation (16 meV) based on the Landau levels formation at high field magneto-absorption.[31] The estimation of binding energy and dielectric constant is within the range of previously reported values for the low-temperature orthorhombic phase of $CH_3NH_3PbI_3$.[47] The obtained E_B value also justifies the use of exciton-related PL emission at cryogenic temperatures (since the thermal fluctuation is ~0.3 meV at 4K).

From the measured spectral difference between the σ- and σ+ emission bands, we obtained the Zeeman splitting, $\Delta E(B)$ ($=g_{ex}\mu_B B$) vs. B as shown in Fig. 2d. The measured $\Delta E(B)$ response clearly shows a linear dependence with B having a maximum value of ~1.5 meV at B=17.5 T. From $\Delta E(B)$ response we evaluate the exciton g-factor, g_{ex}=1.32 for the orthorhombic phase of $CH_3NH_3PbI_3$.[29] Recall that for exciton $g_{ex} = g_e + g_h$ and therefore both g values may deviate considerably from the free electron g-factor of 2.002, due to the strong SOC in this hybrid perovskite.

In the exciton picture of the PL in $CH_3NH_3PbI_3$ using the **k·p** effective-mass approximation,[38] the four e-h spin 1/2 pair configurations are divided into four exciton states with eigenfunctions ψ_1, ψ_2 and two $\psi_5^{\pm}$. ψ_1 is a dark state that does not luminesce; ψ_2 emits linearly polarized light; and only the two $\psi_5^{\pm}$ excitons emit circularly polarized PL. From the model calculation the Zeeman splitting in the Faraday configuration is determined by $g_{ex}=g_{e\parallel}+g_{h\parallel}$, where the anisotropic g-factors are directed along the crystal axis. Alternatively, $g_{e\perp}$ and $g_{h\perp}$ are the anisotropic g-factors of electron and hole in the Voigt configuration. This model predicts the g-factors for holes as $g_{h\parallel}$=-0.472 and $g_{h\perp}$=-0.354, and for electrons $g_{e\parallel}$=1.672 and $g_{e\perp}$=2.281, which agrees well with the recent experimental results using picosecond transient Kerr rotation ($g_{h\perp}$=-0.33, $g_{e\perp}$=2.63).[39] Using the relation $g_{ex}=g_{e\parallel}+g_{h\parallel}$ in the Faraday configuration we get from the model calculation g_{ex}=1.2, also in very good agreement with our result (g_{ex}=1.32).

We now turn to the field-induced circularly polarization (FICPO) value, P, which is defined by the relation P=[PL(σ+)-PL(σ-)]/[PL(σ+)+PL(σ-)]. In general the steady state PL intensity, I from an exciton state at field B is given by:

$$I = \frac{\nu_R}{\nu_R + \nu_{NR}} n(B,T)N, \quad (2)$$

where ν_R is the radiative recombination rate (which is proportional to the transition oscillator strength), ν_{NR} is the non-radiative recombination rate, n(*B*,*T*) is the occupation probability at field *B* and temperature *T* that follows the Boltzmann statistics, and N is the total exciton density under steady state conditions. According to the effective-mass model the radiative transition rate ν_R of ψ_5^+ and ψ_5^- exciton states is the same, and stays roughly the same upon the application of the field.[38] Taking the same ν_{NR} value for ψ_5^+ and ψ_5^- states, the relative intensities of σ- and σ+ PL bands would depend only on n(*B*,*T*). Following the Boltzmann distribution in thermal equilibrium, the relative occupation of ψ_5^+ and ψ_5^- states is given by $n(B,T) \sim \exp(-\Delta E(B)/k_B T)$, where k_B is the Boltzmann constant and ΔE(*B*) is the Zeeman energy splitting from Eq.(1). Since the spin relaxation time is much longer for electrons than holes,[18,39] this prevents the electron spins to reach thermal equilibrium before recombination sets in. We thus believe that the PL circular polarization, which is proportional to the difference in the σ- and σ+ PL intensities is determined by the Zeeman splitting of holes in the VB, $\Delta E_h(B)$ that would introduce a population imbalance, followed by PL emission intensity imbalance that leads to FICPO.

As shown in Fig. 3b, the PL emission of $CH_3NH_3PbI_3$ film shows large FICPO value, *P* at 4K. The difference ΔPL=PL(σ+)-PL(σ-) is plotted in a 2D graph in Fig. 3c. The maximum ΔPL value occurs at a slightly shorter wavelength than the PL emission peak due to the spin splitting between σ- and σ+ emissions. Importantly ΔPL is positive over the entire main emission band. This means that the intensity PL(σ+)>PL(σ-) although the photon energy E(σ+)>E(σ-), and according to the Boltzmann statistics the occupation number density is supposed to be n(σ+)< n(σ-). This 'anomaly' originates from, and *actually validates* the negative *g*-factor of holes in the VB that is due to the strong SOC in $CH_3NH_3PbI_3$.[38,39]

By decomposing the PL spectra into three Lorentzian spectral components and integrating the intensities of the individual components, the field dependent circular polarization, *P*(*B*) of the PL emission from the free exciton is shown in Fig. 3d. The phonon replica shows a similar *P*(*B*) response, but the trap-related PL emission is much

less polarized; i.e. P<2% at 17.5 T (see Fig. S3).[41] Based on the Boltzmann thermal distribution of spin polarized holes in the VB, the estimated P_{th} value is

$$P_{th}(B) = \frac{\exp(\Delta E/kT)-1}{\exp(\Delta E/kT)+1} = \tanh\left(\frac{g_{h\|}\mu_B B}{2kT}\right) \quad (3)$$

However it may be that the spin population does not completely thermalize during the exciton lifetime. In fact the population distribution of the exciton spin sublevels is governed by the *competition* between the spin-lattice relaxation time, τ_s and the recombination lifetime, $\tau=1/(\nu_R+\nu_{NR})$. In this case the circular polarization, P is smaller than P_{th} by a decreasing factor, D (i.e., $P=D\cdot P_{th}$) where $D=\tau/(\tau+\tau_s)$. We note that D~1 if the spin relaxation is extremely fast (τ_s is very short) so that the spin states could reach complete thermal distribution. This is the reason that spin-polarized electrons contribute very little to the circularly polarized PL, as τ_s(e) is one order of magnitude longer than τ_s(h).[18,39] We can get a good fit with the $P(B)$ response in Fig. 3d using Eq.(3) multiplied by D = 0.3 (see Fig. 3d). From this D value we thus obtained τ_s/τ~2 at 4 K for holes in $CH_3NH_3PbI_3$.

To further verify that the obtained FICPO is governed by a partial thermal equilibrium, we measured the circular polarization $P(B$=17.5 T) vs. temperature, T in the range of 4 to 150 K,[48] as shown in Fig. 4a. We note that P decreases sharply with T, especially in the range of T<50 K; this is obvious in spite of the change in PL wavelengths and intensities as seen in Fig. 4a. In Fig. 4b we show $P(B$=17.5 T) vs. temperature compared with the predicted value, P_{th} using Eq.(3) without involving a decreasing-factor. It is clear that using Eq.(3) with a temperature independent D does not fit the data. For example a decreasing factor of D = 0.3 may fit $P(B$=17.5 T) at 4 K (Fig. 3d) but this would substantially deviate from the measured $P(B$=17.5 T) values at high temperatures. This allows to extract additional information from the measured $P(B$=17.5 T) vs T. From the deviation of the measured P value and P_{th} value calculated from Eq.(3) at each temperature we evaluated the decreasing factor vs. temperature, D(T), and subsequently obtained the τ_s/τ ratio vs. T from D(T) (Fig. 4b inset). We note that τ_s/τ shows a steep exponential decrease with T in the range of T<50 K.

It should be mentioned that trions, or called charged excitons may also give rise to unusual FICPO properties, as was previously observed in III-V quantum wells.[49-51] Very recently, the luminescent charged exciton was confirmed to exist in the inorganic perovskite $CsPbBr_3$ quantum dots by high field magneto-optical measurement.[22,23] However, in the polycrystalline thin film of $CH_3NH_3PbI_3$, where the crystal grains are usually hundreds of nanometers, no direct evidence has been shown that charged exciton significantly contributes to the PL emission,[52-54] probably due to the lack of quantum confinement and the balanced photogeneration of electrons/holes. We note in passing that even if the charged excitons were involved in the PL emission, the obtained "anomalous" FICPO would still be explained by a negative *g*-factor of holes, although the *g*-factors of holes and electrons may need to be re-calculated in this case.

In conclusion the steady-state measurements of the field induced circular polarization emission provides a promising method to estimate τ_s from τ values, because the circular polarization follows the Boltzmann distribution that is modified by the competition between the spin relaxation time, τ_s and exciton recombination time, τ. We conclude that the high-field magneto-optical spectroscopy studies in $CH_3NH_3PbI_3$ show the influence of strong SOC on the spin-polarized electronic band structure in hybrid perovskites, which is one of the requirements for spin manipulation with potential in spintronics device applications.

We gratefully thank Drs. E. Ehrenfreund, E. Lafalce and R. McLaughlin for fruitful discussions. This work was supported by the Department of Energy Office of Science, grant DE-SC0014579. The fabrication facility was supported by the National Science Foundation-Material Science & Engineering Center (NSF-MRSEC) program at the University of Utah, grant DMR 1121252. A portion of this work was performed at the National High Magnetic Field Laboratory in Tallahassee FL, which is supported by National Science Foundation Cooperative Agreement No. DMR-1157490 and the State of Florida.

References

(1) A. Kojima, K. Teshima, Y. Shirai, and T. Miyasaka, Organometal halide perovskites as visible-light sensitizers for photovoltaic cells. *J. Am. Chem. Soc.* **131**, 6050 (2009).

(2) J. Burschka, N. Pellet, S.-J. Moon, R. Humphry-Baker, P. Gao, M. K. Nazeeruddin, and M. Grätzel, Sequential deposition as a route to high-performance perovskite-sensitized solar cells. *Nature* **499**, 316 (2013).

(3) D. P. McMeekin, G. Sadoughi, W. Rehman, G. E. Eperon, M. Saliba, M. T. Hörantner, A. Haghighirad, N. Sakai, L. Korte, B. Rech, M. B. Johnston, L. M. Herz, and H. J. Snaith, A mixed-cation lead mixed-halide perovskite absorber for tandem solar cells. *Science* **351**, 151 (2016).

(4) H. Cho, S.-H. Jeong, M.-H. Park, Y.-H. Kim, C. Wolf, C.-L. Lee, J. H. Heo, A. Sadhanala, N. Myoung, S. Yoo, S. H. Im, R. H. Friend, and T.-W. Lee, Overcoming the electroluminescence efficiency limitations of perovskite light-emitting diodes. *Science* **350**, 1222 (2015).

(5) J. Even, L. Pedesseau, J.-M. Jancu, and C. Katan, Importance of Spin–Orbit Coupling in Hybrid Organic/Inorganic Perovskites for Photovoltaic Applications. *J. Phys. Chem. Lett.* **4**, 2999 (2013).

(6) A. Amat, E. Mosconi, E. Ronca, C. Quarti, P. Umari, M. K. Nazeeruddin, M. Grätzel, and F. D. Angelis, Cation-Induced Band-Gap Tuning in Organohalide Perovskites: Interplay of Spin–Orbit Coupling and Octahedra Tilting. *Nano Lett.* **14**, 3608 (2014).

(7) F. Zheng, L. Z. Tan, S. Liu, and A. M. Rappe, Rashba Spin–Orbit Coupling Enhanced Carrier Lifetime in $CH_3NH_3PbI_3$. *Nano Lett.* **15**, 7794 (2015).

(8) W. Gao, X. Gao, T. A. Abtew, Y.-Y. Sun, S. Zhang, and P. Zhang, Quasiparticle band gap of organic-inorganic hybrid perovskites: Crystal structure, spin-orbit coupling, and self-energy effects. *Phys. Rev. B* **93**, 085202 (2016).

(9) C. Zhang, D. Sun, C.-X. Sheng, Y. X. Zhai, K. Mielczarek, A. Zakhidov, and Z. V. Vardeny. Magnetic field effects in hybrid perovskite devices. *Nat. Phys.* **11**, 427-434 (2015).

(10) Y.-C. Hsiao, T. Wu, M. Li, and B. Hu, Magneto-Optical Studies on Spin-Dependent Charge Recombination and Dissociation in Perovskite Solar Cells. *Adv. Mater.* **27**, 2899-2906 (2015).

(11) J. Li, and P. M. Haney, Optical spintronics in organic-inorganic perovskite photovoltaics. *Phys. Rev. B* **93**, 155432 (2016).

(12) D. Sun, C. Zhang, M. Kavand, K. J. van Schooten, H. Malissa, M. Groesbeck, R. McLaughlin, C. Boehme, and Z. V. Vardeny, Spintronics of organometal trihalide perovskites. *arXiv preprint* arXiv: 1608.00993 (2016).

(13) M. Kim, J. Im, A. J. Freeman, J. Ihm, and H. Jin, Switchable S= 1/2 and J= 1/2 Rashba bands in ferroelectric halide perovskites. *PNAS U.S.A.* **111**, 6900 (2014).

(14) M. Kepenekian, R. Robles, C. Katan, D. Sapori, L. Pedesseau, and J. Even, Rashba and Dresselhaus effects in hybrid organic–inorganic perovskites: From basics to devices. *ACS Nano* **9**, 11557 (2015).

(15) D. Niesner, M. Wilhelm, I. Levchuk, A. Osvet, S. Shrestha, and M. Batentschuk, Giant Rashba Splitting in $CH_3NH_3PbBr_3$ Organic-Inorganic Perovskite. *Phys. Rev. Lett.* **117**, 126401 (2016).

(16) E. M. Hutter, M. C. Gélvez-Rueda, A. Osherov, V. Bulović, F. C. Grozema, S. D. Stranks, and T. J. Savenije, Direct–indirect character of the bandgap in methylammonium lead iodide perovskite. *Nat. Mater.* **16**, 115 (2017).

(17) Y. Zhai, S. Baniya, C. Zhang, J. Li, P. Haney, C.-X. Sheng, E. Ehrenfreund, and Z. V. Vardeny, Giant Rashba splitting in 2D organic-inorganic halide perovskites measured by transient spectroscopies. *Sci. Adv.* **3**, e1700704 (2017).

(18) D. Giovanni, H. Ma, J. Chua, M. Grätzel, R. Ramesh, S. Mhaisalkar, N. Mathews, and T. C. Sum, Highly spin-polarized carrier dynamics and ultralarge photoinduced magnetization in $CH_3NH_3PbI_3$ perovskite thin films. *Nano Lett.* **15**, 1553 (2015).

(19) D. Giovanni, W. K. Chong, H. A. Dewi, K. Thirumal, I. Neogi, R. Ramesh, S. Mhaisalkar, N. Mathews, and T. C. Sum, Tunable room-temperature spin-selective optical Stark effect in solution-processed layered halide perovskites. *Sci. Adv.* **2**, e1600477 (2016).

(20) J. Even, L. Pedesseau, C. Katan, M. Kepenekian, J.-S. Lauret, D. Sapori, and E. Deleporte, Solid-state physics perspective on hybrid perovskite semiconductors. *J. Phys. Chem. C* **119**, 10161 (2015).

(21) M. Isarov, L. Z. Tan, M. I. Bodnarchuk, M. V. Kovalenko, A. M. Rappe, and E. Lifshitz, Rashba Effect in a Single Colloidal $CsPbBr_3$ Perovskite Nanocrystal Detected by Magneto-Optical Measurements. *Nano Lett.* **17**, 8, 5020-5026 (2017).

(22) M. Fu, P. Tamarat, H. Huang, J. Even, A. L. Rogach, and B. Lounis, Neutral and Charged Exciton Fine Structure in Single Lead Halide Perovskite Nanocrystals Revealed by Magneto-optical Spectroscopy. *Nano Lett.* **17**, 2895-2901 (2017).

(23) D. Canneson, E. V. Shornikova, D. R. Yakovlev, T. Rogge, A. A. Mitioglu, M. V. Ballottin, P. C. M. Christianen, E. Lhuillier, M. Bayer, and L. Biadala, Negatively Charged and Dark Excitons in $CsPbBr_3$ Perovskite Nanocrystals Revealed by High Magnetic Fields. *Nano Lett.* **17**, 6177-6183 (2017).

(24). M. A. Becker, R. Vaxenburg, G. Nedelcu, P. C. Sercel, A. Shabaev, M. J. Mehl, J. G. Michopoulos, S. G. Lambrakos, N. Bernstein, J. L. Lyons, T. Stöferle, R. F. Mahrt, M. V. Kovalenko, D. J. Norris, G. Rainò, and A. L. Efros, Bright triplet excitons in caesium lead halide perovskites. *Nature* **553**, 189-193 (2018).

(25) D. T. Pierce, and F. Meier, Photoemission of spin-polarized electrons from GaAs. *Phys. Rev. B* **13**, 5484 (1976).

(26) M. J. Snelling, G. P. Flinn, A. S. Plaut, R. T. Harley, A. C. Tropper, R. Eccleston, and C. C. Phillips, Magnetic *g* factor of electrons in GaAs/$Al_xGa_{1-x}As$ quantum wells. *Phys. Rev. B* 34, 11345 (1991).

(27) M. Furis, H. Htoon, M. A. Petruska, V. I. Klimov, T. Barrick, and S. A. Crooker, Bright-exciton fine structure and anisotropic exchange in CdSe nanocrystal quantum dots. *Phys. Rev. B* **73**, 241313(R) (2006).

(28) M. Furis, J. A. Hollingsworth, V. I. Klimov, and S. A. Crooker, Time- and Polarization-Resolved Optical Spectroscopy of Colloidal CdSe Nanocrystal Quantum Dots in High Magnetic Fields. *J. Phys. Chem. B* **109**, 15332 (2005).

(29) M. Hirasawa, T. Ishihara, T. Goto, K. Uchida, and N. Miura, Magnetoabsorption of the lowest exciton in perovskite-type compound $(CH_3NH_3)PbI_3$. *Physica B: Condensed Matter* **201**, 427 (1994).

(30) K. Tanaka, T. Takahashi, T. Ban, T. Kondo, K. Uchida, and N. Miura, Comparative study on the excitons in lead-halide-based perovskite-type crystals $CH_3NH_3PbBr_3$ $CH_3NH_3PbI_3$. *Solid State Commun.* **127**, 619 (2003).

(31) A. Miyata, A. Mitioglu, P. Plochocka, O. Portugall, J. T.-W. Wang, S. D. Stranks, H. J. Snaith, and R. J. Nicholas, Direct measurement of the exciton binding energy and effective masses for charge carriers in organic-inorganic tri-halide perovskites. *Nat. Phys.* **11**, 582 (2015).

(32) K. Galkowski, A. Mitioglu, A. Miyata, P. Plochocka, O. Portugall, G. E. Eperon, J. T.-W. Wang, T. Stergiopoulos, S. D. Stranks, H. J. Snaith, and R. J. Nicholas, Determination of the exciton binding energy and effective masses for methylammonium and formamidinium lead tri-halide perovskite semiconductors. *Energy Environ. Sci.* **9**, 962 (2016).

(33) E. Menéndez-Proupin, P. Palacios, P. Wahnón, and J. C. Conesa, Self-consistent relativistic band structure of the $CH_3NH_3PbI_3$ perovskite. *Phys. Rev. B* **90**, 045207 (2014).

(34) Y. Wang, T. Gould, J. F. Dobson, H. Zhang, H. Yang, X. Yao, and H. Zhao, Density functional theory analysis of structural and electronic properties of orthorhombic perovskite $CH_3NH_3PbI_3$. *Phys. Chem. Chem. Phys.* **16**, 1424 (2014).

(35) Z.-G. Yu, Excitons in Orthorhombic and Tetragonal Hybrid Organic–Inorganic Perovskites. *J. Phys. Chem. C* **121**, 3156 (2017).

(36) R. Kotlyar, T. L. Reinecke, M. Bayer, and A. Forchel, Zeeman spin splittings in semiconductor nanostructures. *Phys. Rev. B* **63**, 085310 (2001).

(37) J. Van Bree, A. Y. Silov, P. Koenraad, M. Flatté, and C. Pryor, *g* factors and diamagnetic coefficients of electrons, holes, and excitons in InAs/InP quantum dots. *Phys. Rev. B* **85**, 165323 (2012).

(38) Z.-G. Yu, Effective-mass model and magneto-optical properties in hybrid perovskites. *Sci. Rep.* **6**, 28576 (2016).

(39) P. Odenthal, W. Talmadge, N. Gundlach, R. Wang, C. Zhang, D. Sun, Z.-G. Yu, Z. V. Vardeny, and Y. S. Li, Spin-polarized exciton quantum beating in hybrid organic-inorganic perovskites. *Nat. Phys.* **13**, 894 (2017).

(40) M. Bayer, A. Kuther, A. Forchel, A. Gorbunov, V. B. Timofeev, F. Schäfer, J. P. Reithmaier, T. L. Reinecke, and S. N. Walck, Electron and hole *g* factors and exchange interaction from studies of the exciton fine structure in $In_{0.60}Ga_{0.40}As$ quantum dots. *Phys. Rev. Lett.* **82**, 1748.

(41) See Supplemental Material at [URL will be inserted by publisher] for experimental details and additional figures.

(42) J. M. Richter, F. Branchi, F. V. de Almeida Camargo, B. Zhao, R. H. Friend, G. Cerullo, and F. Deschler, Ultrafast carrier thermalization in lead iodide perovskite probed with two-dimensional electronic spectroscopy. *Nat. Commun.* **8**, 376 (2017).

(43) M. I. Dar, G. Jacopin, S. Meloni, A. Mattoni, N. Arora, A. Boziki, S. M. Zakeeruddin, U. Rothlisberger, and M. Grätzel, Origin of unusual bandgap shift and dual emission in organic-inorganic lead halide perovskites. Sci. Adv. **2**, e1601156 (2016).

(44) A. D. Wright, C. Verdi, R. L. Milot, G. E. Eperon, M. A. Pérez-Osorio, H. J. Snaith, F. Giustino, M. B. Johnston, and L. M. Herz, Electron–phonon coupling in hybrid lead halide perovskites. Nat. Commun. **7**, 11755 (2016).

(45) L. Q. Phuong, Y. Nakaike, A. Wakamiya, and Y. Kanemitsu, Free Excitons and Exciton–Phonon Coupling in $CH_3NH_3PbI_3$. Single Crystals Revealed by Photocurrent and Photoluminescence Measurements at Low Temperatures. *J. Phys. Chem. Lett.* 7, 4905 (2016).

(46) C. Wehrenfenning, M. Liu, H. J. Snaith, M. B. Johnston, and L. M. Herz, Charge carrier recombination channels in the low temperature phase of organic-inorganic lead halide perovskite thin films. APL Materials **2**, 081513 (2014).

(47) Z. Yang, A. Surrente, K. Galkowski, N. Bruyant, D. K. Maude, A. A. Haghighirad, H. J. Snaith, P. Plochocka, and R. J. Nicholas, Unraveling the exciton binding energy and the dielectric constant in single-crystal methylammonium lead triiodide perovskite. *J. Phys. Chem. Lett.* **8**, 1851-1855 (2017).

(48) It should be noted that a small temperature-independent background of <1% has been removed from the $P(T)$ data points, which could be from the mixing of lower and higher CB bands at very high fields.

(49) K. Kheng, R. T. Cox, Merle Y. d' Aubigné, Franck Bassani, K. Saminadayar, and S. Tatarenko, Observation of Negatively Charged Excitons X^- in Semiconductor Quantum Wells. *Phys. Rev. Lett.* **71**, 1752 (1993).

(50) M. Hayne, C. L. Jones, R. Bogaerts, C. Riva, A. Usher, F. M. Peeters, F. Herlach, V. V. Moshchalkov, and M. Henini, Photoluminescence of negatively charged excitons in high magnetic fields. *Phys. Rev. B* **59**, 2927 (1999).

(51) G. Finkelstein, H. Shtrikman, and I. Bar-Joseph, Negatively and positively charged excitons in $GaAs/Al_xGa_{1-x}As$ quantum wells. *Phys. Rev. B* **53**, R1709(R) (1996).

(52) S. D. Stranks, V. M. Burlakov, T. Leijtens, J. M. Ball, A. Goriely, and H. J. Snaith, Recombination Kinetics in Organic-Inorganic Perovskites: Excitons, Free Charge, and Subgap States. *Phys. Rev. Applied* **2**, 034007 (2014).

(53) K. Wu, A. Bera, C. Ma, Y. Du, Y. Yang, L. Li, and T. Wu, Temperature-dependent excitonic photoluminescence of hybrid organometal halide perovskite films. *Phys. Chem. Chem. Phys.* **16**, 22476-22481 (2014).

(54) H.-H. Fang, R. Raissa, M. Abdu-Aguye, S. Adjokatse, G. R. Blake, J. Even, and M. A. Loi, Photophysics of organic-inorganic hybrid lead iodide perovskite single crystals. *Adv. Funct. Mater.* **25**, 2378-2385 (2015).

Figure Captions

FIG. 1. (Color online) The PL emission measurements from the $CH_3NH_3PbI_3$ film at low temperature. (a) Experimental apparatus for measuring the high-field circularly polarized PL emission. (b) The photoexcitation species in $CH_3NH_3PbI_3$ that include photocarriers, free excitons (and their phonon replica), and excitons trapped in shallow traps. (c) The PL emission spectrum from $CH_3NH_3PbI_3$ film at T=4 K, which is decomposed into three emission bands: namely free exciton, phonon replica and trapped exciton. The fitting is based on multi-peak Lorentzian functions.

FIG. 2. (Color online) Zeeman-type spin splitting in $CH_3NH_3PbI_3$ determined by the circularly polarized PL emission at high magnetic field. (a) Schematic illustration of the radiative recombination in $CH_3NH_3PbI_3$ between spin sublevels of electrons in the CB and holes in the VB. (b) Normalized σ+ and σ- circularly polarized PL emission spectra at 4 K measured at B=0 and B=17.5 T, respectively, which show a field-induced splitting between two transitions. (c) Plots of the central wavelength of the two free exciton polarized PL bands at various fields B, showing both Zeeman splitting and diamagnetic blue-shift. (d) Energy splitting, ΔE between the σ+ and σ- PL bands vs. B up to 17.5 T measured at 4 K.

FIG. 3. (Color online) Field-induced circular polarization in the PL emission of $CH_3NH_3PbI_3$ film. (a) Schematic illustration of the relaxation and recombination processes between spin sublevels of electrons in the CB and holes in the VB. The thermal spin distribution of holes in the VB introduces unequal PL intensities with σ- and σ+ polarizations. Note that the hole g-factor is negative in $CH_3NH_3PbI_3$. (b) Field-induced circularly polarized PL emission bands (σ+ and σ-, red and blue lines, respectively) from $CH_3NH_3PbI_3$ film measured at 4 K and B=17.5 T. (c) False color plot of the difference, ΔPL of the circular polarized PL spectra (ΔPL= PL(σ+)-PL(σ-)) at various B fields. (d) The circular polarization value, P vs. B for the free exciton band (black squares), and a fit using Eq.(3) without (black line) or with (red line) a decreasing factor, D = 0.3.

FIG. 4. (Color online) The temperature dependence of the PL circular polarization in $CH_3NH_3PbI_3$ film at high magnetic field. (a) False color plot of the PL circular

polarization value, *P* at *B*=17.5 T as a function of temperature, *T* between 4 to 150 K. (b) The *P* value for the free exciton PL band measured at *B*=17.5 T at various temperatures (black squares), compared with a theoretical prediction based on Eq.(3) with constant *D* (red line). Inset: the ratio of the spin relaxation time to the recombination time, τ_s/τ vs. temperature extracted from fitting the *P* value at each temperature, with suitable *D* using Eq.(3) (black squares). The red line is an exponential fit for T<50 K.

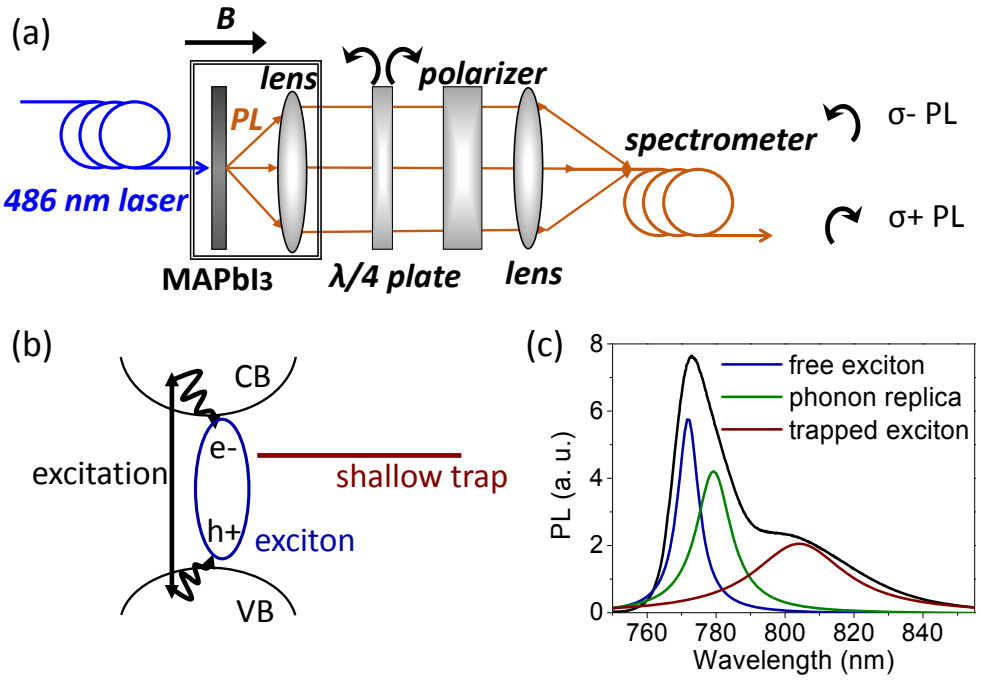

FIG. 1. The PL emission measurements from the $CH_3NH_3PbI_3$ film at low temperature. (a) Experimental apparatus for measuring the high-field circularly polarized PL emission. (b) The photoexcitation species in $CH_3NH_3PbI_3$ that include photocarriers, free excitons (and their phonon replica), and excitons trapped in shallow traps. (c) The PL emission spectrum from $CH_3NH_3PbI_3$ film at T=4 K, which is decomposed into three emission bands: namely free exciton, phonon replica and trapped exciton. The fitting is based on multi-peak Lorentzian functions.

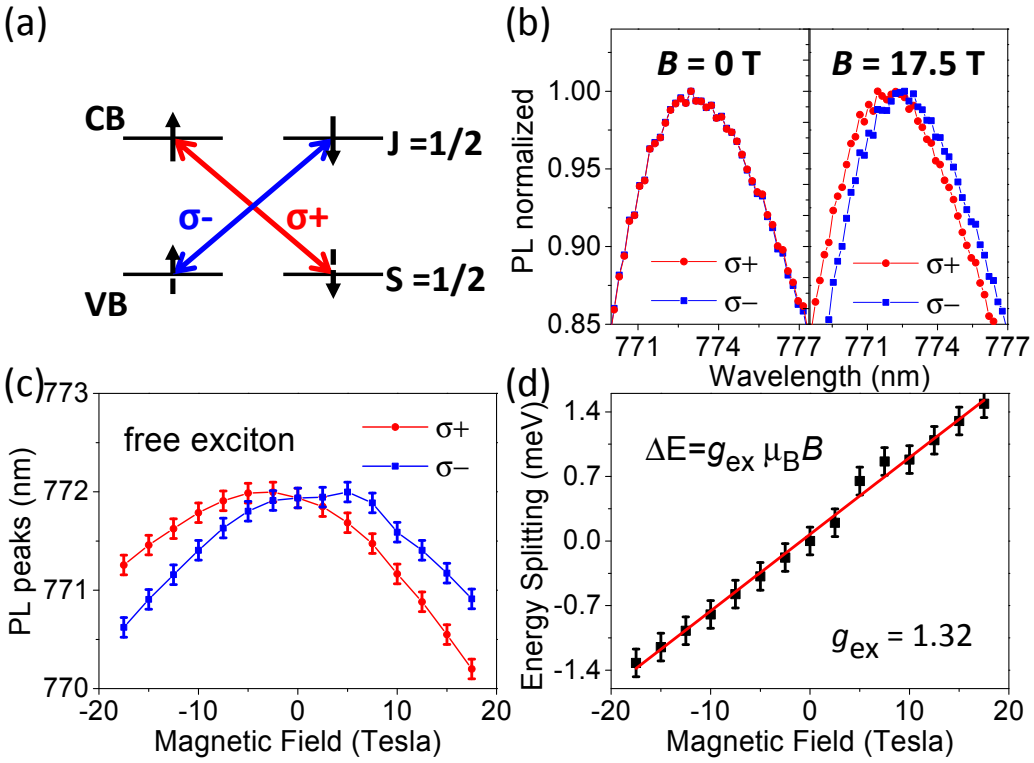

FIG. 2. Zeeman-type spin splitting in $CH_3NH_3PbI_3$ determined by the circularly polarized PL emission at high magnetic field. (a) Schematic illustration of the radiative recombination in $CH_3NH_3PbI_3$ between spin sublevels of electrons in the CB and holes in the VB. (b) Normalized σ+ and σ- circularly polarized PL emission spectra at 4 K measured at B=0 and B=17.5 T, respectively, which show a field-induced splitting between two transitions. (c) Plots of the central wavelength of the two free exciton polarized PL bands at various fields B, showing both Zeeman splitting and diamagnetic blue-shift. (d) Energy splitting, ΔE between the σ+ and σ- PL bands vs. B up to 17.5 T measured at 4 K.

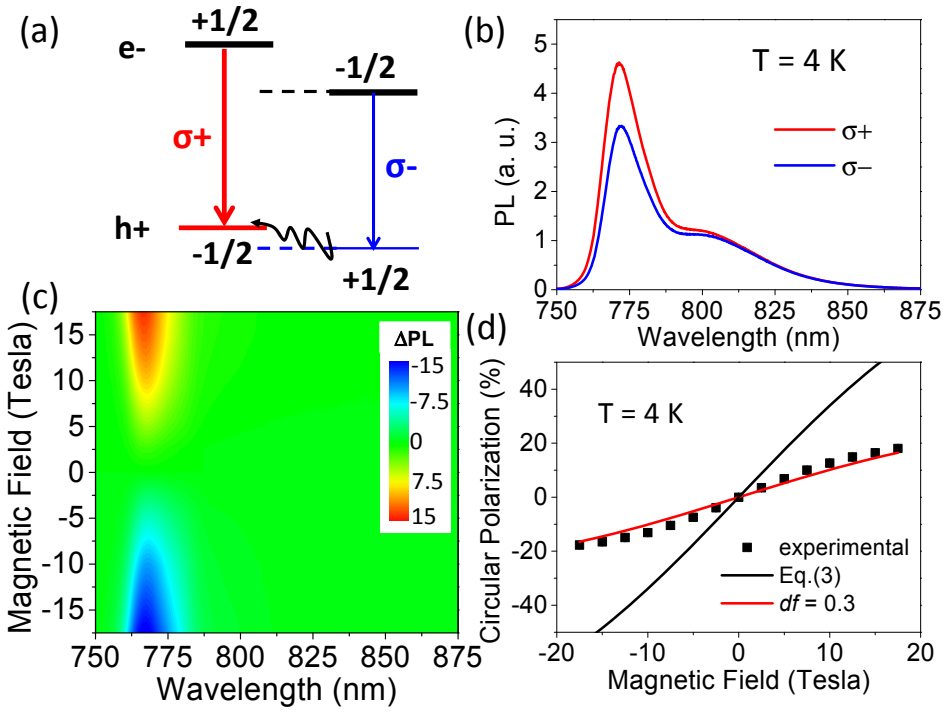

FIG. 3. Field-induced circular polarization in the PL emission of $CH_3NH_3PbI_3$ film. (a) Schematic illustration of the relaxation and recombination processes between spin sublevels of electrons in the CB and holes in the VB. The thermal spin distribution of holes in the VB introduces unequal PL intensities with σ- and σ+ polarizations. Note that the hole *g*-factor is negative in $CH_3NH_3PbI_3$. (b) Field-induced circularly polarized PL emission bands (σ+ and σ-, red and blue lines, respectively) from $CH_3NH_3PbI_3$ film measured at 4 K and B=17.5 T. (c) False color plot of the difference, ΔPL of the circular polarized PL spectra (ΔPL= PL(σ+)-PL(σ-)) at various B fields. (d) The circular polarization value, P vs. B for the free exciton band (black squares), and a fit using Eq.(3) without (black line) or with (red line) a decreasing factor, D = 0.3.

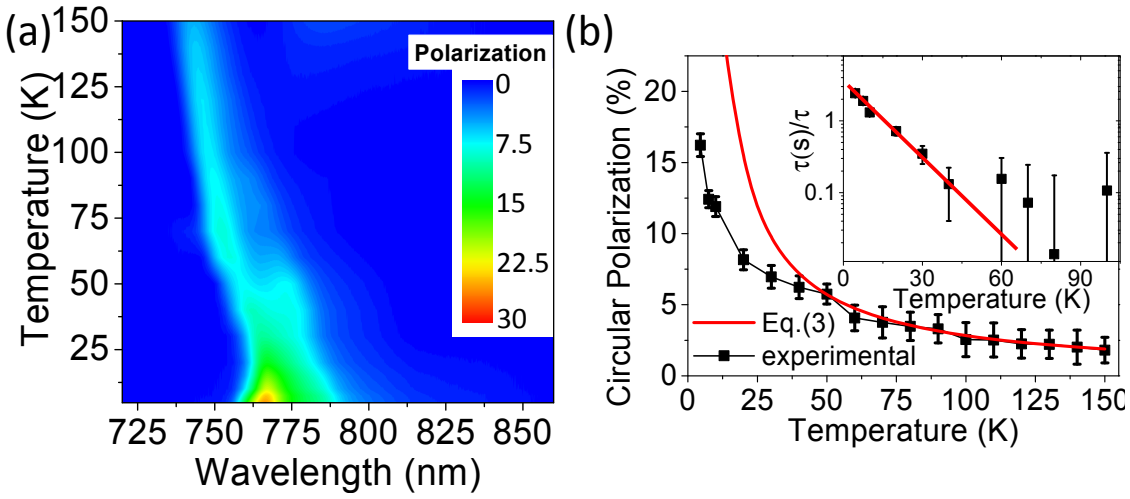

FIG. 4. The temperature dependence of the PL circular polarization in $CH_3NH_3PbI_3$ film at high magnetic field. (a) False color plot of the PL circular polarization value, *P* at *B*=17.5 T as a function of temperature, *T* between 4 to 150 K. (b) The *P* value for the free exciton PL band measured at *B*=17.5 T at various temperatures (black squares), compared with a theoretical prediction based on Eq.(3) with constant *D* (red line). Inset: the ratio of the spin relaxation time to the recombination time, τ_s/τ vs. temperature extracted from fitting the *P* value at each temperature, with suitable *D* using Eq.(3) (black squares). The red line is an exponential fit for T<50 K.